The Astrophysical Journal Letters, 999:L14 (6pp), 2026 March 1 https://doi.org/10.3847/2041-8213/ae36a2
© 2026. The Author(s). Published by the American Astronomical Society.
OPEN ACCESS

Upper Limit on HF(1–0) Absorption in a Dusty Star-forming Galaxy at $z = 6$: Constraints on Early Fluorine Enrichment

Akiyoshi Tsujita[1], Chiaki Kobayashi[2,3], Yuki Yoshimura[1], Kotaro Kohno[1,4], Ken-ichi Tadaki[5], Fumiya Maeda[6], Hideki Umehata[7,8], Shuo Huang[8,9], Bunyo Hatsukade[9,10,11], Fumi Egusa[1], Kana Morokuma-Matsui[1], Yoichi Tamura[8], and Yuri Nishimura[12,13,14]

[1] Institute of Astronomy, Graduate School of Science, The University of Tokyo, 2-21-1 Osawa, Mitaka, Tokyo 181-0015, Japan
[2] Kavli Institute for the Physics and Mathematics of the Universe (WPI), The University of Tokyo Institutes for Advanced Study, The University of Tokyo, Kashiwa, Chiba 277-8583, Japan
[3] Centre for Astrophysics Research, Department of Physics, Astronomy and Mathematics, University of Hertfordshire, Hatfield, AL10 9AB, UK
[4] Research Center for the Early Universe, Graduate School of Science, The University of Tokyo, 7-3-1 Hongo, Bunkyo-ku, Tokyo 113-0033, Japan
[5] Faculty of Engineering, Hokkai-Gakuen University, Toyohira-ku, Sapporo 062-8605, Japan
[6] Research Center for Physics and Mathematics, Osaka Electro-Communication University, 18-8 Hatsucho, Neyagawa, Osaka 572-8530, Japan
[7] Institute for Advanced Research, Nagoya University, Furocho, Chikusa, Nagoya 464-8602, Japan
[8] Department of Physics, Graduate School of Science, Nagoya University, Furocho, Chikusa, Nagoya 464-8602, Japan
[9] National Astronomical Observatory of Japan, 2-21-1 Osawa, Mitaka, Tokyo 181-8588, Japan
[10] Department of Astronomy, Graduate School of Science, The University of Tokyo, 2-21-1 Osawa, Mitaka, Tokyo 181-0015, Japan
[11] Graduate Institute for Advanced Studies, SOKENDAI, Osawa, Mitaka, Tokyo 181-8588, Japan
[12] Institute of Pure and Applied Sciences, University of Tsukuba, 1-1-1 Tennodai, Tsukuba, Ibaraki, 305-8577, Japan
[13] Tomonaga Center for the History of the Universe, University of Tsukuba, 1-1-1 Tennodai, Tsukuba, Ibaraki, 305-8577, Japan
[14] Tsukuba Institute for Advanced Research (TIAR), University of Tsukuba, 1-1-1 Tennodai, Tsukuba, Ibaraki, 305-8577, Japan
Received 2025 December 10; revised 2026 January 9; accepted 2026 January 9; published 2026 February 27

Abstract

Wolf–Rayet (WR) stars have recently attracted attention as possible drivers of early chemical enrichment, including the production of fluorine, whose nucleosynthetic origin remains debated. To test the contribution of massive stars to fluorine production in the early Universe, we conducted Atacama Large Millimeter/submillimeter Array Band 5 spectroscopy of the HF(1–0) absorption line toward a dusty star-forming galaxy at $z = 6.024$. This galaxy has a known gas-phase metallicity and is too young for low-mass asymptotic giant branch stars to have contributed significantly, providing a clean environment to isolate massive-star yields. We do not detect significant HF absorption ($\sim 2\sigma$) and derive a conservative 5σ upper limit of $N_{\rm HF}/N_{\rm H_2} < 2.2 \times 10^{-9}$. This limit is about an order of magnitude below typical local measurements, indicating inefficient fluorine enrichment $\sim$0.9 Gyr after the Big Bang. Comparison with chemical evolution models shows that our constraint is consistent with scenarios without WR yields at this epoch. Expanding the sample of HF absorption measurements in high-redshift galaxies with well-characterized metallicities will be crucial for tracing the onset of WR enrichment and fluorine production across cosmic time.

Unified Astronomy Thesaurus concepts: Chemical abundances (224); Starburst galaxies (1570); High-redshift galaxies (734); Millimeter-wave spectroscopy (2252); Strong gravitational lensing (1643)

1. Introduction

Recent discoveries of unusually high N/O ratios in high-redshift galaxies have drawn attention to Wolf–Rayet (WR) stars as a possible driver of early chemical enrichment (e.g., A. J. Bunker et al. 2023; Y. Isobe et al. 2023; C. Kobayashi & A. Ferrara 2024; D. A. Berg et al. 2025). Another element that it has been suggested that WR stars contribute to the production of is fluorine (M. Franco et al. 2021). Fluorine (^{19}F) is one of the few elements whose nucleosynthetic origin and evolution are still much debated. Its unusually low cosmic abundance compared to neighboring elements indicates that standard stellar nucleosynthesis largely bypasses fluorine, making it a sensitive probe of nonstandard stellar yields (e.g., N. Ryde et al. 2020). Theoretically, three astrophysical objects have been considered as the primary sources of ^{19}F production: asymptotic giant branch (AGB) stars, WR stars, and core-collapse supernovae (SNe II) with the neutrino process. Among them, AGB stars are the only observationally confirmed producers (e.g., A. Jorissen et al. 1992; K. Werner et al. 2005; M. Otsuka et al. 2008; C. Abia et al. 2010, 2015; S. Lucatello et al. 2011), and low-mass AGB stars ($\sim$2–4 $M_\odot$) are considered the main contributors to ^{19}F production at solar metallicity (e.g., M. Lugaro et al. 2004; A. I. Karakas 2010; C. Kobayashi et al. 2011b; K. A. Womack et al. 2023). However, AGB yields alone cannot reproduce the observed fluorine abundances in the solar neighborhood, implying additional contributions from massive stars such as WR stars and SNe II (e.g., A. Renda et al. 2004; C. Kobayashi et al. 2011a, 2020; H. Jönsson et al. 2014; N. Prantzos et al. 2018; E. Spitoni et al. 2018; N. Ryde et al. 2020). Although non-AGB contributions are expected, direct tests are scarce, mainly because fluorine tracers are limited to the vibrational–rotational HF lines in the infrared and the rotational transitions in the millimeter regime, the latter being inaccessible to local stars. The vibrational–rotational HF lines are difficult to detect in extremely metal-poor stars, limiting stellar fluorine measurements to a small number of carbon-enhanced objects (e.g., A. Mura-Guzmán et al. 2020). This is primarily because most metal-poor stars have sufficiently high effective

Original content from this work may be used under the terms of the Creative Commons Attribution 4.0 licence. Any further distribution of this work must maintain attribution to the author(s) and the title of the work, journal citation and DOI.

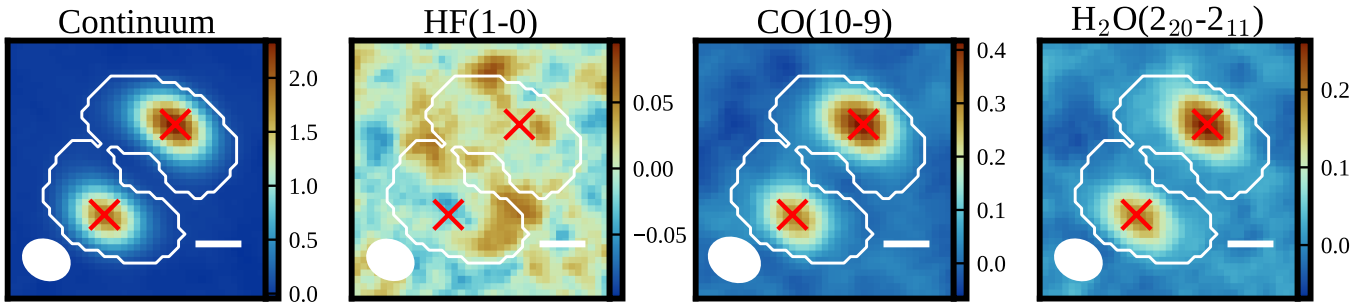

Figure 1. ALMA continuum and velocity-integrated (moment-0) maps of G09.83808. From left to right: dust continuum at ∼170 GHz, HF(1–0) absorption, CO(10–9), and $H_2O(2_{20}–2_{11})$ lines. White contours indicate the clean mask. Red crosses mark the two continuum peaks used for line spectrum extraction and photometry. The synthesized beam is shown as a white ellipse in the lower left of each panel. White scale bars indicate 1″, which corresponds to 5.7 kpc. The colorbar units are mJy beam^{-1} for the continuum and mJy beam^{-1} km s^{-1} for the lines.

temperatures to dissociate HF molecules. Moreover, such observations probe the photospheric ^{19}F abundance of individual stars rather than the element already ejected into the interstellar medium (ISM), leaving the efficiency of ^{19}F ejection uncertain.

A complementary approach is to probe fluorine in the ISM of young but already metal-rich galaxies, where AGB enrichment is still limited but short-lived massive stars can operate efficiently. Recently, M. Franco et al. (2021) serendipitously detected the HF(1–0) absorption line in a lensed dusty star-forming galaxy (DSFG) at $z = 4.4$, about 1.4 Gyr after the Big Bang, when the contribution from low-mass AGB stars is expected to be small. Their chemical-evolution models showed that this could be explained either by including yields from WR stars or by assuming a short starburst timescale ($\tau_{\rm SF}$∼0.1 Gyr) even without WR contributions. However, the lack of constraints on the galaxy's star formation history and metallicity left this degeneracy unresolved. To take the next step, ideal targets for HF absorption are bright DSFGs at high redshift with metallicity measurements. While the James Webb Space Telescope (JWST) has significantly improved constraints on the mass–metallicity relation up to z∼10, especially for low- to intermediate-mass galaxies (e.g., K. Nakajima et al. 2023; R. L. Sanders et al. 2024; A. Sarkar et al. 2025), the relation remains poorly constrained at the high-mass end ($M_\star \gtrsim 10^{10}\,M_\odot$), although recent work has begun to explore this regime (e.g., A. L. Faisst et al. 2025). In addition, estimating stellar masses of DSFGs is difficult due to severe dust attenuation, requiring deep JWST observations. Owing to this combination, high-redshift massive DSFGs with well-determined metallicities remain rare.

Among the few most distant, bright DSFGs known at $z > 6$, G09.83808 at $z = 6.024$, corresponding to a cosmic age of only ∼0.9 Gyr after the Big Bang (J. A. Zavala et al. 2018; A. Tsujita et al. 2022), provides the best opportunity to extend such studies. This DSFG has gas-phase metallicity already enriched to $Z \approx 0.5$–$0.7\,Z_\odot$, as inferred from the $[\mathrm{N\,II}]_{205\mu\mathrm{m}}/[\mathrm{O\,III}]_{88\mu\mathrm{m}}$ luminosity ratio combined with far-infrared continuum flux density ratio (K. Tadaki et al. 2022). In addition, this DSFG benefits from strong lensing ($\mu \sim 8$–9; K. Tadaki et al. 2022) and lies on the massive end of the star-forming main sequence (J. A. Zavala et al. 2022), offering a more representative view of typical $z \sim 6$ massive galaxies compared to the other two known extreme DSFGs at $z > 6$, which are intrinsically much brighter ($S_{870\mu\mathrm{m,intr}} > 10$ mJy) and reside in protocluster environments (D. A. Riechers et al. 2013; D. P. Marrone et al. 2018). In this Letter, we present Atacama Large Millimeter/submillimeter Array (ALMA) HF(1–0) absorption line observations toward G09.83808, aiming to investigate early fluorine production.

This Letter is organized as follows. Section 2 describes the observations and data reduction. Section 3 presents the HF absorption analysis and the derived fluorine abundance constraint. In Section 4, we compare our observational constraints with a chemical-evolution model. Throughout the Letter, we adopt a cosmology with $\Omega_{\rm m} = 0.3$, $\Omega_\Lambda = 0.7$, and $H_0 = 70\,\mathrm{km\,s^{-1}\,Mpc^{-1}}$ and the Kroupa initial mass function (P. Kroupa 2001).

2. Observations and Data Reduction

Our ALMA Band 5 observations of G09.83808 were conducted between 2024 October and December during Cycle 10–11 (Project code: 2023.1.01281.S; PI: A. Tsujita). We targeted the HF(1–0) absorption line ($\nu_{\rm rest} = 1232.48$ GHz; $\nu_{\rm obs} = 175.47$ GHz at $z = 6.024$), covering ∼161.7–175.8 GHz in the 4 bit mode. The observations were carried out in multiple scheduling blocks using the C43-3/4/5 antenna configurations. All datasets were calibrated using the standard ALMA pipeline in the `CASA` package (CASA Team et al. 2022). Continuum subtraction was performed with the `uvcontsub` task, carefully selecting line-free channels for each tuning. We first created a clean mask from the continuum map imaged with Briggs weighting (robust parameter of 0.0), using the `auto-multithresh` algorithm (A. A. Kepley et al. 2020). This clean mask was then reused for all line cubes (white contours in Figure 1). Line imaging was carried out using the `tclean` task with natural weighting, adopting a cell size of 0.″15 and cleaning down to `nsigma=2`. The final spectral cube has a synthesized beam of $1.''2 \times 0.''96$ and an rms noise of 0.08 mJy beam^{-1} per 50 km s^{-1} channel at the frequency of the HF(1–0) line. Velocity-integrated maps were created by integrating over ±300 km s^{-1} around the expected line center.

Figure 1 shows the dust continuum map and the continuum-subtracted velocity-integrated maps of the HF(1–0), CO(10–9), and $H_2O(2_{20}–2_{11})$ lines. Given the modest angular resolution, the lensed image is resolved into two arcs in the continuum map. We extract a single-beam spectrum at the peak pixel of each arc in the continuum image (red cross marks in Figure 1) and sum them channel by channel to form the total spectrum. For each channel, the 1σ uncertainty is estimated from the rms measured in blank regions outside the source. Figure 2 presents the continuum-subtracted spectrum centered on the systemic velocity, binned to 50 km s^{-1}. For comparison, we overlay the

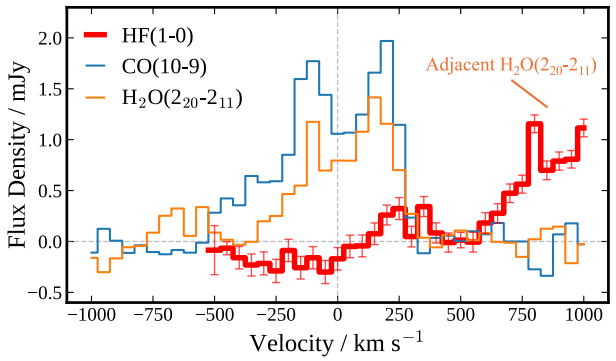

Figure 2. Continuum-subtracted spectra centered on the systemic velocity. The HF(1–0) absorption line (red) is shown with 1σ error bars and binned to 50 km s^{-1}. For comparison, the CO(10–9) (blue) and $H_2O(2_{20}$–$2_{11})$ (orange) lines from the same dataset are overlaid. We note that the positive feature near +800 km s^{-1} in the HF spectrum is the adjacent $H_2O(2_{20}$–$2_{11})$ line.

HF(1–0) absorption line with the CO(10–9) (blended with $H_2O(3_{12}$–$2_{21})$) and the $H_2O(2_{20}$–$2_{11})$ lines from the same dataset.

3. Results

We calculate the fluorine abundance from the obtained spectrum. As shown in Figure 2, a tentative HF(1–0) absorption feature is seen near the systemic velocity, with a peak depth of -0.30 ± 0.08 mJy (3.8σ) at -50 km s^{-1}. We define the integration range using the unblended $H_2O(2_{11}$–$2_{02})$ line, selecting channels with $>1\sigma$ signal, which yields [–300, +300] km s^{-1}. Within this range, the HF(1–0) velocity-integrated flux is -43 ± 20 mJy km s^{-1} (2.2σ). Given the modest signal-to-noise ratio, we conservatively treat this measurement as an upper limit in the analysis below. For reference, we also calculate the integrated flux over [−450, 0] km s^{-1} where the HF signal itself exceeds 1σ, which yields -97 ± 17 mJy km s^{-1} (5.7σ). However, using either this value or the 5σ upper limit adopted below does not affect our main conclusions. The continuum level, measured at the same two pixels and summed in the same way, is 4.24 ± 0.02 mJy.

Because the HF $J = 1$ level has an extremely high critical density of $n_{\rm crit} \sim 10^{10}$ cm^{-3} at $T = 50$ K (D. A. Neufeld et al. 2005), essentially all HF resides in the ground state and the $J = 1$–0 absorption traces the total HF column density. The HF column density can therefore be obtained from the velocity-integrated optical depth using the relation given by D. A. Neufeld et al. (2010):

$$\int \tau(v)\, dv = 4.16 \times 10^{-13} N_{\rm HF}\ {\rm cm^2\ km\ s^{-1}}.$$

Applying this relation to the 5σ flux limit yields $N_{\rm HF} < 6.0 \times 10^{14}$ cm^{-2} (5σ). However, we note that this upper limit may still underestimate the true HF abundance, because (1) the continuum emission may not fully illuminate all absorbing clouds along the line of sight, (2) only gas in front of the continuum source contributes to the absorption, and (3) any HF in excited states is not accounted for.

Next, we constrain the HF abundance ratio by estimating the molecular hydrogen column density as follows. Using the intrinsic molecular gas mass $(2.0 \pm 0.7) \times 10^{10}\, M_\odot$ from the CO(2–1) line (J. A. Zavala et al. 2022), together with a CO-to-H_2 conversion factor of $\alpha_{\rm CO} = 1.0\, M_\odot$ (K km s^{-1} pc^2)$^{-1}$,

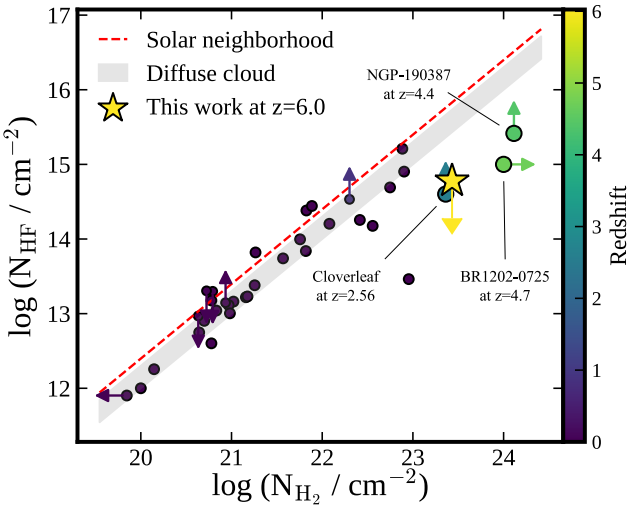

Figure 3. HF column density versus H_2 column density. Literature measurements of HF in absorption and emission (circles; D. A. Neufeld et al. 2010; T. G. Phillips et al. 2010; P. Sonnentrucker et al. 2010; R. R. Monje et al. 2011a; M. Emprechtinger et al. 2012; J. Kamenetzky et al. 2012; N. Indriolo et al. 2013; M. Pereira-Santaella et al. 2013; K. Kawaguchi et al. 2016; N. Lu et al. 2017; Ü. Kavak et al. 2019) are color coded by redshift, and the new measurement from this work is shown as a star. Arrows indicate upper and lower limits. The red dashed line denotes the fluorine abundance in the solar neighborhood (F/H = 2.5×10^{-8}; E. Maiorca et al. 2014), and the black dotted line shows the typical $N_{\rm HF}/N_{\rm H_2}$ value found in Galactic diffuse molecular clouds ((1–2) $\times 10^{-8}$; e.g., P. Sonnentrucker et al. 2010). Three high-redshift sources are highlighted for comparison: the DSFG NGP-190387 at $z = 4.4$ (M. Franco et al. 2021), the QSO BR1202−0725 at $z = 4.7$, where HF is detected in emission (M. D. Lehnert et al. 2020), and the QSO Cloverleaf at $z = 2.56$ (R. R. Monje et al. 2011b).

a CO excitation ratio of $r_{21} = 0.83 \pm 0.10$ (M. S. Bothwell et al. 2013), and assuming the gas follows the $[{\rm C\,II}]_{158\mu{\rm m}}$ distribution with a half-light radius of ∼1 kpc (A. Tsujita et al. 2026, in preparation), we obtain $N_{\rm H_2} = 2.7 \times 10^{23}$ cm^{-2}. The corresponding abundance limit is $N_{\rm HF}/N_{\rm H_2} < 2.2 \times 10^{-9}$ or $\log_{10}(N_{\rm HF}/N_{\rm H_2}) < -8.7$ (5σ). We adopt an $\alpha_{\rm CO}$ value commonly used for local ULIRGs (e.g., D. Downes & P. M. Solomon 1998). For G09.83808, dynamical constraints suggest $\alpha_{\rm CO} < 2.5\, M_\odot$ (K km s^{-1} pc^2)$^{-1}$ (J. A. Zavala et al. 2022). Adopting a larger $\alpha_{\rm CO}$ would increase $N_{\rm H_2}$ and thus decrease $N_{\rm HF}/N_{\rm H_2}$, so our qualitative conclusions below remain unchanged.

Because HF forms efficiently via the exothermic reaction $F + H_2 \rightarrow HF + H$ and is resistant to destruction under typical interstellar conditions, it is expected to be the dominant gas-phase reservoir of fluorine wherever hydrogen is predominantly molecular (e.g., C. Zhu et al. 2002). Consequently, the abundance ratio $N_{\rm HF}/N_{\rm H_2}$ provides a sensitive empirical indicator of fluorine enrichment. Figure 3 places our constraint in this context by comparing it with HF detections and limits in the Milky Way, nearby galaxies, and high-redshift galaxies/quasars. In the solar neighborhood, the fluorine abundance is A(F) = 12 + log(F/H) = 4.40, corresponding to F/H = 2.5×10^{-8} (number ratio; E. Maiorca et al. 2014),[15] which provides an approximate upper bound on $N_{\rm HF}/N_{\rm H_2}$ if nearly all fluorine is locked in HF. Observations of diffuse molecular clouds in the Milky Way yield slightly lower ratios, $N_{\rm HF}/N_{\rm H_2} \sim (1 - 2) \times 10^{-8}$ (e.g., P. Sonnentrucker et al. 2010).

[15] An earlier determination based on a different excitation potential of the vibrational–rotational HF line reported A(F) = 4.56, corresponding to F/H = 3.6×10^{-8} (M. Asplund et al. 2009).

At low molecular columns ($N_{H_2} \lesssim 10^{22.5}\,cm^{-2}$), these measurements follow a relatively tight correlation between N_{HF} and N_{H_2}. At higher N_{H_2} and toward higher redshift (R. R. Monje et al. 2011b; M. D. Lehnert et al. 2020; M. Franco et al. 2021), the relation becomes less clear, showing larger scatter and a possible flattening around $N_{HF} \sim 10^{15}\,cm^{-2}$. Our 5σ upper limit for G09.83808 also lies below these reference values, extending fluorine abundance constraints to $z = 6$.

4. Discussion and Conclusion

To interpret our HF constraint, we compare it with the galactic chemical-evolution model of C. Kobayashi et al. (2020), which is also adopted by M. Franco et al. (2021). This model self-consistently includes fluorine production from all plausible sources, namely AGB stars (including super-AGB stars), SNe II (including hypernovae), and rotationally enhanced WR winds; the neutrino process in C. Kobayashi et al. (2011a) is uncertain and is *not* included. Therefore, fluorine is enhanced in AGB and WR stars by He burning. The inclusion of the rotating massive stars is a key feature, as stellar rotation enhances internal mixing and mass loss, enabling the ejection of fluorine even at lower stellar masses ($\gtrsim 20 M_\odot$) and metallicities.

The yields are taken from M. Limongi & A. Chieffi (2018), adopting a rotation velocity of $v_{rot} = 300\,km\,s^{-1}$ for all stars with initial masses of 13–120 $M_\odot$; this represents a maximum WR contribution, since such a high rotation speed is applied uniformly across all massive stars regardless of metallicity. The fiducial model adopts a Kroupa IMF (a slope of $x = 1.3$ for 0.01–120 $M_\odot$); a more bottom-heavy IMF would increase the relative contribution from AGB stars but suppress that from massive stars, leading to lower total fluorine yields (for a given star formation history, SFH). In galactic chemical-evolution models, the metallicity in the ISM is calculated as a function of time, assuming the formation epoch, the star formation timescale τ_{SF}, and the gas-infall timescale τ_{in}. These model parameters are degenerate and should be constrained from observations, which we do in this Letter. For G09.83808, we have two independent observational constraints, namely the gas-phase metallicity ($Z \approx 0.5$–$0.7\,Z_\odot$; K. Tadaki et al. 2022) and the molecular gas fraction ($f_{gas} \simeq 0.20$; J. A. Zavala et al. 2022). Once the observed gas fraction is imposed, the formation epoch is effectively fixed; in the fiducial solution it corresponds to $z_{form} \sim 8.5$. Adopting $\tau_{in} = 1$ Gyr, the observed metallicity is then reproduced with a star formation timescale of $\tau_{SF} = 0.37$ Gyr. We refer to this combination as our fiducial model. These constraints represent a major improvement over the previous study by M. Franco et al. (2021), for which the star formation history remained largely uncertain. We note that in this fiducial model, the newly produced F from AGB stars is only 0.23% of the total fluorine abundance at $z = 6.02$, indicating that the contribution from AGB stars is negligible at this epoch.

Figure 4 (top panel) compares our observational constraint with the fiducial model predictions. The left panel shows the evolution of oxygen abundance A(O), which serves as a proxy for overall metallicity and is used to anchor each model track to the observed value for G09.83808. The right panel shows the corresponding fluorine abundance A(F). Our 5σ upper limit on HF/H_2 ($<2.2 \times 10^{-9}$) is consistent with the models without WR yields and does not require additional fluorine production from massive stars.

To assess the robustness of this result, we explore variations in the model parameters, as illustrated in Figure 4. First of all, reducing the rotation velocity of massive stars from 300 to $150\,km\,s^{-1}$ produces negligible changes in both the oxygen and fluorine evolution tracks (top panel). Second, we examine models with different star formation and infall timescales (middle panel). When the observed metallicity and gas fraction are imposed, changing τ_{SF} simply requires a compensating change in τ_{in}, and all such combinations converge to the same fluorine abundance. Thus the predicted A(F) is insensitive to variations in the SFH under these constraints. Finally, we vary the IMF slope (bottom panel). Changing the Kroupa IMF slope from $x = 1.3$ to either $x = 1.1$ (top heavy) or $x = 1.7$ (bottom heavy) yields modest differences in fluorine abundance ($\sim$0.1–0.4 dex), but the resulting oxygen abundance A(O) fails to match the observed metallicity. After adjusting τ_{SF} to reproduce $Z \approx 0.5$–$0.7\,Z_\odot$, the predicted A(F) converges back to the fiducial track. Taken together, these tests demonstrate that the low HF abundance in G09.83808 cannot be explained with WR stars, even varying stellar rotation velocity, SFH, or IMF slope. With both the metallicity and gas fraction independently known, the fluorine abundance becomes a direct probe of the underlying nucleosynthesis, allowing us to place strong constraints on the contribution of WR stars at $z > 6$.

We discuss possible explanations for the low HF abundance observed in G09.83808. First, partial depletion of HF onto dust grains could in principle lower the observed HF column density, particularly in dense, cold environments where freeze-out becomes efficient (e.g., M. H. D. van der Wiel et al. 2016). However, the relatively high dust temperature ($T_{dust} = 51 \pm 4$ K; K. Tadaki et al. 2022) and the elevated cosmic microwave background temperature at $z = 6$ ($T_{CMB} = 19.2$ K) render freeze-out inefficient under typical ISM densities ($n_H \sim 10^3$–$10^4\,cm^{-3}$). Following the arguments of M. Franco et al. (2021), such high dust and radiation temperatures significantly shorten the thermal desorption timescale relative to the freeze-out timescale, making it unlikely that a significant fraction of HF is locked onto dust grains.

Second, the galaxy may be observed during a particular phase in an intermittent SFH, a scenario proposed to explain elevated N/O ratios in high-redshift galaxies (e.g., C. Kobayashi & A. Ferrara 2024). In this framework, after the initial starburst, secondary gas inflow dilutes the ISM and triggers a secondary starburst, from which WR stars cause high (N, F)/O. Then, SNe II dominate to decrease (N, F)/(O, Fe) ratios until the onset of AGB enrichment. In fact, Figure 4 of C. Kobayashi & A. Ferrara (2024) shows that [F/Fe] declines sharply during this postburst phase. If G09.83808 were in the SNe II enrichment phase, its high metallicity and low fluorine abundance would be naturally explained.

Third, the WR fluorine yields themselves remain highly uncertain, depending on model assumptions such as mass-loss rates, convection, magnetic field, and the way to include rotation (e.g., M. Limongi & A. Chieffi 2018).

By contrast, the $z = 4.4$ galaxy studied by M. Franco et al. (2021) exhibits a much higher HF abundance. Within the similar chemical-evolution framework, such a value can be reproduced either by including rotation-enhanced WR yields or by adopting a very short star formation timescale

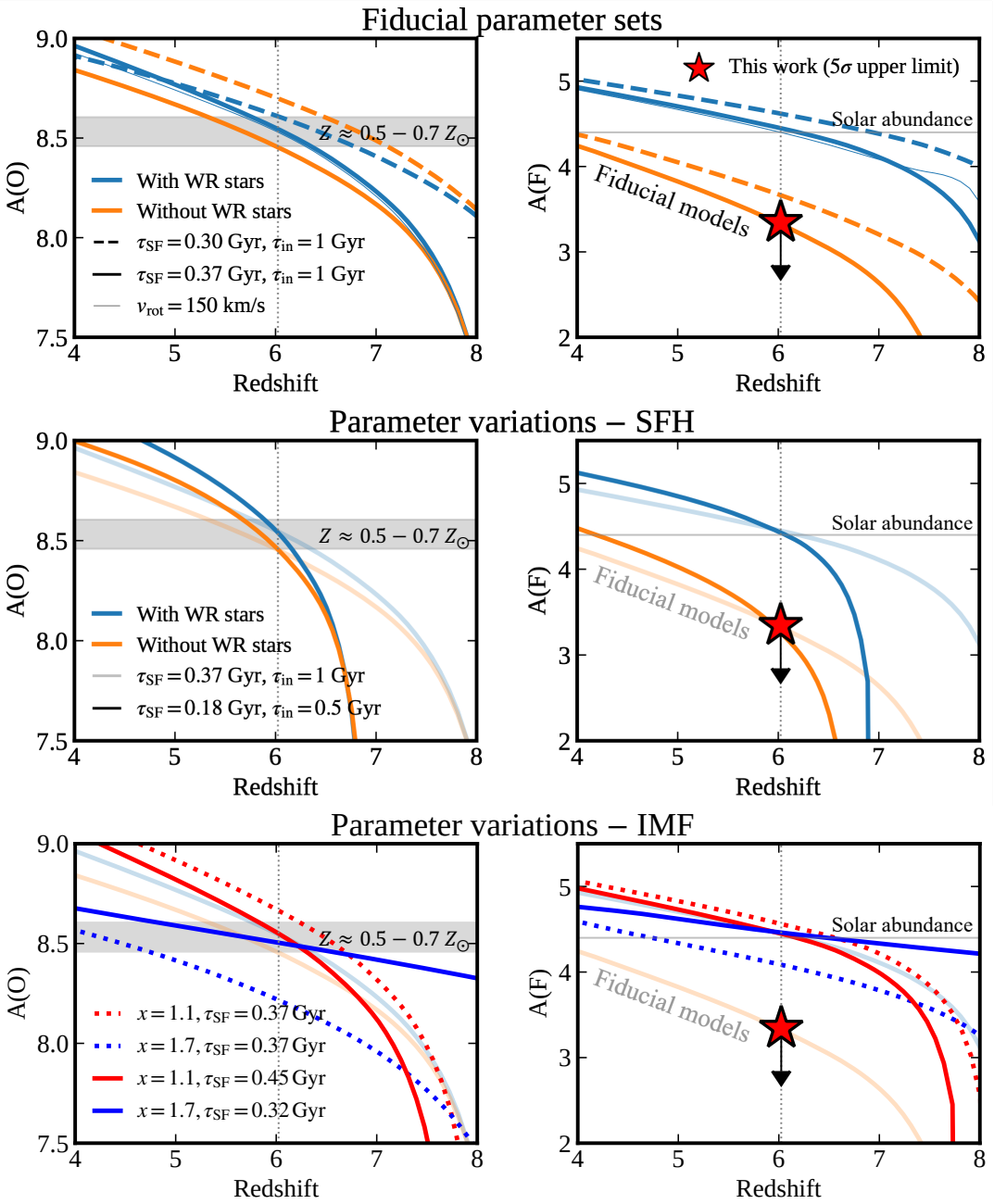

Figure 4. Predicted evolution of the oxygen abundance A(O) (left) and fluorine abundance A(F) (right) for chemical-evolution models constrained to reproduce the observed metallicity of G09.83808 ($Z \approx 0.5$–$0.7\ Z_\odot$; K. Tadaki et al. 2022), shown as the gray band in the A(O) panel and its gas fraction ($f_{gas} = 0.2$; J. A. Zavala et al. 2022). (Top) Fiducial models, all of which assume a Kroupa IMF with slope $x = 1.3$. WR-included cases adopt a stellar rotation velocity of $v_{rot} = 300$ km s^{-1} except for the thin line. Blue and orange curves denote models with and without WR yields, respectively. The solid curves show the model with $\tau_{SF} = 0.37$ Gyr and $\tau_{in} = 1$ Gyr, while the dashed curves adopt $\tau_{SF} = 0.3$ Gyr. A slower-rotation WR model ($v_{rot} = 150$ km s^{-1}, blue thin curve) is shown for comparison and differs only slightly from the 300 km s^{-1} WR model. The vertical dotted line marks $z = 6.024$. In the A(F) panel, the gray horizontal line shows the solar abundance (E. Maiorca et al. 2014), and the red star marks our 5σ upper limit. This limit is consistent with models without WR enrichment and with longer star formation timescales. (Middle) Models with different star formation and infall timescales. The bold curves show an alternative SFH ($\tau_{SF} = 0.18$ Gyr, $\tau_{in} = 0.5$ Gyr) that also satisfies the observed metallicity and gas-fraction constraints, while the faint curves are the fiducial models. To satisfy the constraints, the models yield nearly identical A(F) regardless of the adopted timescales. (Bottom) Models exploring variations in the IMF slope. The dotted lines adopt IMF slopes of $x = 1.1$ (red) and $x = 1.7$ (blue) while keeping all other parameters at the fiducial values; these models fail to reproduce the observed metallicity. The solid red and blue curves retune the star formation timescale to $\tau_{SF} = 0.45$ and 0.32 Gyr, respectively, so that the models match the observed metallicity, in which case the predicted A(F) remains similar to the fiducial case.

($\tau_{SF} \sim 0.1$ Gyr). However, due to the lack of independent constraints on the galaxy's metallicity or SFH, the model remained degenerate in that case. Our result for G09.83808 breaks this degeneracy and reveals that WR-driven fluorine production was not yet efficient for this case. The discrepancy between these two galaxies may reflect diversity in star formation modes, enrichment histories, or WR activity among early galaxies. Expanding the sample of HF absorption measurements in high-redshift galaxies with known metallicities will be crucial to trace the onset and evolution of fluorine production from massive stars across cosmic time.

Acknowledgments

We thank the anonymous referee and the editor for constructive and insightful comments, which helped improve the clarity and quality of this manuscript. Data analysis was in part carried out on the Multi-wavelength Data Analysis System operated by the Astronomy Data Center (ADC), NAOJ. This research was supported by FoPM, WINGS Program, the University of Tokyo. A.T. acknowledges the support by JSPS KAKENHI grant No. JP24KJ0562. C.K. acknowledge funding from the UK Science and Technology Facilities Council through grant ST/Y001443/1. K.K. acknowledges the support by JSPS KAKENHI grant Nos. JP22H04939, JP23K20035, and JP24H00004. F.M. is supported by JSPS KAKENHI grant No. JP23K13142. H.U. is supported by JSPS KAKENHI grant No. 25K01039. Y.N. acknowledges support from JSPS KAKENHI grant Nos. JP23K13140 and JP23K20035. This Letter makes use of the following ALMA data: ADS/JAO. ALMA #2023.1.01281.S. ALMA is a partnership of ESO (representing its member states), NSF (USA) and NINS (Japan), together with NRC (Canada), NSTC, and ASIAA (Taiwan), and KASI (Republic of Korea), in cooperation with the Republic of Chile. The Joint ALMA Observatory is operated by ESO, AUI/NRAO, and NAOJ.

Author Contributions

A.T. led the project, including the proposal preparation, data analysis, and manuscript writing. C.K. constructed the chemical-evolution models. C.K., Y.Y., K.K., K.T., and F.M. provided overall support throughout the project. All authors contributed to discussions and the improvement of the manuscript.

Facility: ALMA.

Software: Astropy (Astropy Collaboration et al. 2022), Numpy (C. R. Harris et al. 2020), Scipy (P. Virtanen et al. 2020), Matplotlib (J. D. Hunter 2007), CASA (CASA Team et al. 2022).

ORCID iDs

Akiyoshi Tsujita https://orcid.org/0000-0002-0498-5041
Chiaki Kobayashi https://orcid.org/0000-0002-4343-0487
Yuki Yoshimura https://orcid.org/0000-0002-1413-1963
Kotaro Kohno https://orcid.org/0000-0002-4052-2394
Ken-ichi Tadaki https://orcid.org/0000-0001-9728-8909
Hideki Umehata https://orcid.org/0000-0003-1937-0573
Shuo Huang https://orcid.org/0009-0006-1731-6927
Bunyo Hatsukade https://orcid.org/0000-0001-6469-8725
Fumi Egusa https://orcid.org/0000-0002-1639-1515
Kana Morokuma-Matsui https://orcid.org/0000-0003-3932-0952
Yoichi Tamura https://orcid.org/0000-0003-4807-8117
Yuri Nishimura https://orcid.org/0000-0003-0563-067X

References

Abia, C., Cunha, K., Cristallo, S., & de Laverny, P. 2015, A&A, 581, A88
Abia, C., Cunha, K., Cristallo, S., et al. 2010, ApJL, 715, L94
Asplund, M., Grevesse, N., Sauval, A. J., & Scott, P. 2009, ARA&A, 47, 481
Astropy Collaboration, Price-Whelan, A. M., Lim, P. L., et al. 2022, ApJ, 935, 167
Berg, D. A., Naidu, R. P., Chisholm, J., et al. 2025, arXiv:2511.13591
Bothwell, M. S., Smail, I., Chapman, S. C., et al. 2013, MNRAS, 429, 3047
Bunker, A. J., Saxena, A., Cameron, A. J., et al. 2023, A&A, 677, A88
CASA Team, Bean, B., Bhatnagar, S., et al. 2022, PASP, 134, 114501
Downes, D., & Solomon, P. M. 1998, ApJ, 507, 615
Emprechtinger, M., Monje, R. R., van der Tak, F. F. S., et al. 2012, ApJ, 756, 136
Faisst, A. L., Liu, L.-J., Dubois, Y., et al. 2025, arXiv:2510.16106
Franco, M., Coppin, K. E. K., Geach, J. E., et al. 2021, NatAs, 5, 1240
Harris, C. R., Millman, K. J., van der Walt, S. J., et al. 2020, Natur, 585, 357
Hunter, J. D. 2007, CSE, 9, 90
Indriolo, N., Neufeld, D. A., Seifahrt, A., & Richter, M. J. 2013, ApJ, 764, 188
Isobe, Y., Ouchi, M., Tominaga, N., et al. 2023, ApJ, 959, 100
Jönsson, H., Ryde, N., Harper, G. M., et al. 2014, A&A, 564, A122
Jorissen, A., Smith, V. V., & Lambert, D. L. 1992, A&A, 261, 164
Kamenetzky, J., Glenn, J., Rangwala, N., et al. 2012, ApJ, 753, 70
Karakas, A. I. 2010, MNRAS, 403, 1413
Kavak, Ü., van der Tak, F. F. S., Tielens, A. G. G. M., & Shipman, R. F. 2019, A&A, 631, A117
Kawaguchi, K., Muller, S., Black, J. H., et al. 2016, ApJ, 822, 115
Kepley, A. A., Tsutsumi, T., Brogan, C. L., et al. 2020, PASP, 132, 024505
Kobayashi, C., & Ferrara, A. 2024, ApJL, 962, L6
Kobayashi, C., Izutani, N., Karakas, A. I., et al. 2011a, ApJ, 739, L57
Kobayashi, C., Karakas, A. I., & Umeda, H. 2011b, MNRAS, 414, 3231
Kobayashi, C., Karakas, A. I., & Lugaro, M. 2020, ApJ, 900, 179
Kroupa, P. 2001, MNRAS, 322, 231
Lehnert, M. D., Yang, C., Emonts, B. H. C., et al. 2020, A&A, 641, A124
Limongi, M., & Chieffi, A. 2018, ApJS, 237, 13
Lu, N., Zhao, Y., Díaz-Santos, T., et al. 2017, ApJS, 230, 1
Lucatello, S., Masseron, T., Johnson, J. A., Pignatari, M., & Herwig, F. 2011, ApJ, 729, 40
Lugaro, M., Ugalde, C., Karakas, A. I., et al. 2004, ApJ, 615, 934
Maiorca, E., Uitenbroek, H., Uttenthaler, S., et al. 2014, ApJ, 788, 149
Marrone, D. P., Spilker, J. S., Hayward, C. C., et al. 2018, Natur, 553, 51
Monje, R. R., Emprechtinger, M., Phillips, T. G., et al. 2011a, ApJL, 734, L23
Monje, R. R., Phillips, T. G., Peng, R., et al. 2011b, ApJL, 742, L21
Mura-Guzmán, A., Yong, D., Abate, C., et al. 2020, MNRAS, 498, 3549
Nakajima, K., Ouchi, M., Isobe, Y., et al. 2023, ApJS, 269, 33
Neufeld, D. A., Sonnentrucker, P., Phillips, T. G., et al. 2010, A&A, 518, L108
Neufeld, D. A., Wolfire, M. G., & Schilke, P. 2005, ApJ, 628, 260
Otsuka, M., Izumiura, H., Tajitsu, A., & Hyung, S. 2008, ApJL, 682, L105
Pereira-Santaella, M., Spinoglio, L., Busquet, G., et al. 2013, ApJ, 768, 55
Phillips, T. G., Bergin, E. A., Lis, D. C., et al. 2010, A&A, 518, L109
Prantzos, N., Abia, C., Limongi, M., Chieffi, A., & Cristallo, S. 2018, MNRAS, 476, 3432
Renda, A., Fenner, Y., Gibson, B. K., et al. 2004, MNRAS, 354, 575
Riechers, D. A., Bradford, C. M., Clements, D. L., et al. 2013, Natur, 496, 329
Ryde, N., Jönsson, H., Mace, G., et al. 2020, ApJ, 893, 37
Sanders, R. L., Shapley, A. E., Topping, M. W., Reddy, N. A., & Brammer, G. B. 2024, ApJ, 962, 24
Sarkar, A., Chakraborty, P., Vogelsberger, M., et al. 2025, ApJ, 978, 136
Sonnentrucker, P., Neufeld, D. A., Phillips, T. G., et al. 2010, A&A, 521, L12
Spitoni, E., Matteucci, F., Jönsson, H., Ryde, N., & Romano, D. 2018, A&A, 612, A16
Tadaki, K., Tsujita, A., Tamura, Y., et al. 2022, PASJ, 74, L9
Tsujita, A., Tadaki, K.-i., Kohno, K., et al. 2022, PASJ, 74, 1429
van der Wiel, M. H. D., Naylor, D. A., Makiwa, G., Satta, M., & Abergel, A. 2016, A&A, 593, A37
Virtanen, P., Gommers, R., Oliphant, T. E., et al. 2020, NatMe, 17, 261
Werner, K., Rauch, T., & Kruk, J. W. 2005, A&A, 433, 641
Womack, K. A., Vincenzo, F., Gibson, B. K., et al. 2023, MNRAS, 518, 1543
Zavala, J. A., Casey, C. M., Spilker, J., et al. 2022, ApJ, 933, 242
Zavala, J. A., Montaña, A., Hughes, D. H., et al. 2018, NatAs, 2, 56
Zhu, C., Krems, R., Dalgarno, A., & Balakrishnan, N. 2002, ApJ, 577, 795